RSC Advances

ROYAL SOCIETY OF CHEMISTRY

www.rsc.org/advances

Investigation on Temperature Stability Performance of Giant Permittivity (In+Nb) in Co–doped TiO_2 Ceramic: A Crucial Aspect for Practical Electronic Applications

Wattana Tuichai [a], Supamas Danwittayakul [b], Santi Maensiri [c], Prasit Thongbai [a,*]

[a] *Integrated Nanotechnology Research Center (INRC), Department of Physics, Faculty of Science, Khon Kaen University, Khon Kaen 40002, Thailand*

[b] *National Metal and Materials Technology Center, National Science and Technology Development Agency, Thailand Science Park, Pathumthani 12120, Thailand*

[c] *School of Physics, Institute of Science, Suranaree University of Technology, Nakhon Ratchasima 30000, Thailand*

* Corresponding author's Email: pthongbai@kku.ac.th (P. Thongbai)

ABSTRACT

In this work, it was shown that the crucial aspect for practical applications of a newly discovered (In+Nb) co–doped TiO_2 material is the temperature stability of its dielectric permittivity (ε′). Despite an extremely large ε′ value of ≈5.1×10^4 and a low loss tangent (tanδ≈0.03) successfully obtained in 10%(In+Nb) co–doped TiO_2, careful inspection revealed that ε′ was largely changed below room temperature (RT) as a result of an ambient–RT dielectric relaxation, giving rise to a large value of the temperature coefficient. However, this result can be effectively improved by decreasing co–doping concentration. Although this dielectric relaxation also occurred in 2.5%(In+Nb) co–doped TiO_2, its ε′ variation below RT was slight. Notably, very high ε′≈1.57×10^4 and ultra–low tanδ≈0.006 (at 30 ^oC and 10^2 Hz) with an excellent temperature coefficient of less than ±7% in the range of -70–180 ^oC were achieved. The giant ε′ response over a broad temperature range in (In+Nb) co–doped TiO_2 was primarily due to the polarization of highly localized electrons in large defect–dipole clusters. The additional polarization relaxation near the RT range might be associated with interfacial polarization of delocalized electron originating from uncorrelated $Nb_2^{5+}Ti^{3+}A_{Ti}$ defect dipoles.

Keywords: TiO_2, Giant permittivity, Loss tangent, Dielectric relaxation.

1. Introduction

Recently, a large number of giant–dielectric materials with very high dielectric permittivities ($\varepsilon' > 10^3$) have been discovered. They are considered potentially useful in electronic applications such as capacitors and memory devices or in high energy–dense storage applications. These giant–dielectric materials are derived from $CaCu_3Ti_4O_{12}$ and related compounds,[1-3] $\boldsymbol{Ln}_{2-x}Sr_xNiO_4$ (***Ln*** = Nd, La, Sm),[4-7] NiO–based oxides,[8] $\mathbf{A}Fe_{1/2}\mathbf{B}_{1/2}O_3$ (A=Ba, Sr, Ca; B=Nb, Ta, Sb),[9, 10] $LuFe_2O_4$,[11] as well as $BaTiO_3$/Ni composite materials.[12] Unfortunately, the tanδ values of these materials are usually larger than 0.1 in a low frequency range, which are higher than the standard values for capacitor applications. This is a significant impediment to practical electronic applications using these materials. To the best of our knowledge, the temperature stability of ε' ($\Delta\varepsilon'/\varepsilon'_{RT}$ (%)) or temperature coefficient of capacitance ($\Delta C/C_{RT}$ (%)) of these giant dielectric materials is more a difficult problem to solve.[13-15] Large increases in ε' (at 1 kHz) at high temperatures are usually due to DC conduction in the materials and the electrical response of grain boundaries. This is one of the most important parameters used for developing dielectric materials for practical applications in electronic devices. For example, in X7R capacitors, $\Delta\varepsilon'/\varepsilon'_{RT}$ of a dielectric material used must be less than ±15% over the temperature range of -55 to 125 ^oC.[16]

Most recently, Hu *et al.* (2013)[17] reported excellent dielectric properties in a (In+Nb) co–doped rutile–TiO_2 (IN–T) ceramic system. A $(In_{0.5}Nb_{0.5})_xTi_{1-x}O_2$ ceramic with $x = 0.1$, exhibited a very low tanδ≈0.02 and an especially high $\varepsilon' \sim 6\times10^4$ that was frequency independent over the range of 10^2–10^6 Hz. Notably, ε' was independent of temperature over a wide temperature range of 80–450 K (-193–177 ^oC). This excellent dielectric performance was attributed to deliberately introduce large defect–dipole clusters containing highly localized electrons. Using this novel and elegant model, the complex stoichiometry of

$(In_x^{3+}Nb_x^{5+}Ti_x^{3+})Ti_{1-3x}^{4+}O_{2-x/2}$ produced defect clusters, in which the electrons created by Nb^{5+} doping ions resulting in the reduction of Ti^{4+} to Ti^{3+} are contained by the presence of In^{3+}.[18] Without In^{3+}, electrons would be delocalized and lead to high DC conductivity and tanδ values. In the other words, this excellent dielectric performance in IN–T ceramics can be created by engineering the local structure within the rutile–TiO_2 structure.

Generally, the existence of dielectric relaxation in any temperature range is usually accompanied by a rapid change in ε′ and the appearance of a strong tanδ peak.[19] Although the relaxation phenomena in a dielectric can give some important clues to clarify the origin of the dielectric response,[7, 10, 11, 17, 20-22] it may be undesirable for practical applications due to the resulting large changes in dielectric properties. In pioneering work,[17] two primary dielectric relaxations were observed in IN–T ceramics. The main dielectric relaxation was due to freezing electrons in defect–dipoles. This resulted in a giant ε′ that was observed in the temperature range of 10–40 K with activation energies of 0.015–0.02 eV.[17, 20] Another relaxation caused by an extrinsic effect was observed in the range of 450–720 K.[17] Thus, a ε′ plateau between these two relaxations should be independent of temperature from 50 to 450 K if no other dielectric relaxation occurs between these two relaxations. However, a set of small tanδ–peaks (≈240–360 K) likely appeared in the loss spectra of 10%IN–T (Fig. 2(a) of Ref. [17]). This might be another relaxation that occurred at an ambient RT. Although the maximum tanδ value at the relaxation peak was kept low (<0.02),[17] the ε′ values in the vicinity of this relaxation might be greatly changed, giving rise to a large value of $\Delta\varepsilon'/\varepsilon'_{RT}(\%)$. The appearance of this ambient RT–relaxation was further confirmed by Zhao *et al*.[20] This dielectric relaxation (DR3 in Fig. 3(a) of Ref. [20]) was clearly observed in the temperature range of 200–280 K for 5%IN–T.

It is very important to investigate the effect of such ambient RT–dielectric relaxations on the temperature–stability of IN–T ceramics because of the great importance for this parameter for practical applications in electronic devices. To the best our knowledge, the exact values of $\Delta\varepsilon'/\varepsilon'_{RT}$ of IN–T ceramics and other co–doped TiO_2 systems have never been reported and discussed from this point of view.[17, 20, 23-27] Thus, the aim of this work is to study the temperature dependent behavior of IN–T ceramics at two very different dopant levels. This will allow study of the influence of ambient–RT dielectric relaxation on the dielectric properties over a standard temperature range for capacitor applications. We found that substitution of (In+Nb) co–doping ions into TiO_2 at a high concentration can greatly enhance ε' and while successfully achieving a low tanδ value. However, its temperature stability below RT was simultaneously worsened. By reducing the co–dopant concentration, excellent ε' temperature stability was accomplished.

2. Experimental details

$(In_{0.5}Nb_{0.5})_xTi_{1-x}O_2$ ceramics with x=0, 0.025, and 0.10 were prepared using a solid state reaction (SSR) method. This ceramics were referenced as 0%IN–T, 2.5%IN–T, and 10%IN–T samples, respectively. TiO_2 (Sigma–Aldrich, >99.9% purity), Nb_2O_5 (Sigma–Aldrich, 99.99% purity), and In_2O_3 (Sigma–Aldrich, 99.99% purity) were used as the starting raw materials. First, a stoichiometric mixture of the starting materials was ball–milled in ethanol for 24 h using ≈2.0 mm diameter ZrO_2 balls. The mixed powder was ground and pressed into pellets (without a binder) of 9.5 mm in diameter and ≈1.2 mm in thickness by uniaxial compression at ≈200 MPa. Finally, these pellets were sintered at different temperatures (1400–1550 ^oC) for 1–10 h.

X–ray diffraction (XRD; Bruker, D 2phaser) was used to characterize the phase composition and crystal structures of the sintered IN–T ceramics. The microstructure and elemental distribution in the TINO ceramic were examined using a field–emission scanning electron microscopy (FE–SEM) with energy-dispersive X–ray analysis (EDX) (HITACHI SU8030, Japan). Before electrical measurements, Au was sputtered onto each pellet face at a current of 25 mA for 8 min using a Polaron SC500 sputter coating unit (Sussex, UK). The capacitance and dispassion factor (D or tanδ) of the ceramic samples were measured using an Agilent 4294A Precision Impedance Analyzer over the frequency and temperature ranges of 10^2–10^6 Hz and -70–220 ^oC, respectively.

3. Results and discussion

Fig. 1(a) shows the XRD patterns of all sintered IN–T ceramics. A main phase of rutile–TiO_2 (JCPDS 21–1276) was observed in all samples with no impurity phase. The diffraction peaks in all XRD patterns were perfectly indexed based on a tetragonal structure. Lattice parameters were calculated from the diffraction peaks and found to be a=4.593 Å and c=2.960 Å, a=4.598 Å and c=2.965Å, and a=4.613 Å and c=2.977 Å for the 0%IN–T, 2.5%IN–T, and 10%IN–T samples, respectively. As shown in Fig. 1(b), both the a and c parameters increased with increasing co–dopant concentration. The a and c values of the 0%IN–T sample were nearly the same as the sample in values for retile–TiO_2 (JCPDS 21–1276) with a=4.593 Å and c=2.959 Å. It is important to note that a and c values of the 10%IN–T sample were very close to the values reported by Hu *et al.*[17] with a≈4.615 Å and c≈2.980 Å for 10% (In+Nb) co–doped TiO_2 ceramic (see Fig. S7 of Supplementary information of Ref. [17]). The enlarged lattice parameters are likely due to the larger ionic radii

of In^{3+} and Nb^{5+} over that of Ti^{4+}. This clearly indicates that both In^{3+} and Nb^{5+} doping ions can be substituted into the rutile–TiO_2 structure.

Fig. 2 shows the microstructure of the 10%IN–T and 2.5%IN–T samples. It was found that the grain size of IN–T ceramics decreased with increasing co–dopant concentration. The estimated grain sizes of the 0%IN–T, 2.5%IN–T, and 10%IN–T samples were of ≈50–100, ≈25–50, and ≈10–20 μm, respectively. This indicates that the grain growth rate of TiO_2 was inhibited by In^{3+} and Nb^{5+} dopant ions. Furthermore, residual pores were only observed in the microstructure of the 10%IN–T sample. These pores were homogeneously distributed throughout the microstructure and appeared at the grain boundaries and triple junctions between grains, indicating normal grain growth characteristic. Note that, the abnormal grain growth was not observed in all the samples.

Usually, inhomogeneous distribution of dopants is one of the most common factors that result in abnormal grain growth.[28] Thus, it is likely that both In^{3+} and Nb^{5+} doping ions were homogeneously distributed in the TiO_2. To further analyze the distributions of the elements in co–doped TiO_2 ceramics, mapping of all elements, *i.e.*, Ti, O, In, and Nb, was performed. As shown in Fig. 3, the dopants were homogeneously dispersed in both the grain and grain boundary of the 2.5%IN–T sample. This was similar to that observed in the 10%IN–T sample. Segregation of In^{3+} and Nb^{5+} ions at any specific region, such as grain boundaries, was not observed.

It was clearly demonstrated that high–ε′ with low–tanδ values in co–doped TiO_2 will be achieved only if two types of defects caused by In^{3+} and Nb^{5+} dopants overlapped or were separated by less than 5 Å.[17, 18] From the microstructural analysis, the distribution of In^{3+} and Nb^{5+} dopants was very homogenous at the microscopic level. However, the overlap of defect dipoles cannot be completely confirmed. The existence of strongly correlated defect dipoles

that give rise to the high–dielectric performance of IN–T ceramics is likely justified by considering their apparent dielectric parameters. As shown in Fig. 4(a) and its inset, the 10%IN–T sample exhibited a high–ε′, on the order of 10^4–10^5, with a low–frequency tanδ value <0.1. At 10^2 Hz and 30 °C, ε′ and tanδ values were about 5.1×10^4 and 0.03, respectively, confirming strongly correlated defect dipoles. It is notable that these values are comparable to ε′≈6.1×10^4 and tanδ≈0.02 for the 10%IN–T ceramic reported.[17] Slight differences in ε′ and tanδ values may have been due to different sintering conditions, which was demonstrated by Li *et al*.[26] In the temperature range from -60 to 150 °C, ε′ was very slightly dependent on frequency between 10^2–10^6 Hz. The dielectric relaxation, which is usually characterized by a steplike decrease in ε′, was not observed in these dielectric spectra. In the inset of Fig. 4(a), broad tanδ peaks were observed in the temperature range of -30 to 30 °C, signifying that dielectric relaxation occurred. As is clearly illustrated in Fig. 4(b), steplike decreases in ε′ and tanδ peaks were simultaneously observed in the temperature range from -60 to 50 °C for the 10%IN–T sample sintered at 1500 °C for 5 h. The existence of this ambient RT dielectric relaxation is consistent with both the 5% and 10%IN–T ceramics sintered at 1400 °C for 10 h.[17, 20]

It was found that the temperature dependence of the frequency at which the tanδ peak appeared (f_{max}) follows the Arrhenius equation:

$$f_{max} = f_0 \exp(-E_a / k_B T) \ , \qquad (1)$$

where f_0 is the pre–factor, E_a is the activation energy required for the relaxation process, k_B is the Boltzmann constant, and T is absolute temperature. As shown in Fig. 4(c), a good linear fit was achieved. This result indicates a non–polaron type relaxation due to a hopping motion of localized carriers.[17, 21] E_a was calculated from the slope of the fitted line and found

to be 0.551 eV for the 10%IN–T sample. In Fig 4(b), ε′ of the 10%IN–T sample rapidly decreased at temperatures under 0 ^{o}C, while ε′ was still too large (≈4×10^{4}). This resulted in a very large temperature coefficient that is undesirable for electronic applications, especially *X–R* type capacitors. As shown in Fig. 4(d), large values of the temperature coefficient in high and low temperature ranges (zones H and L, respectively) were clearly caused by R_H and R_M, respectively. The condition, $\Delta C/C_{RT} < \pm 15\%$, of the 10%IN–T sample was only achieved in the temperature range of -30 to 170 ^{o}C (zone M).

Despite measurements over a limited temperature range (-70–220 ^{o}C) in the current study, it is likely that there are at least three temperature regions in which dielectric relaxations occurred in the IN–T ceramic system: low (<-70 ^{o}C), middle (an ambient RT, -60 to 50 ^{o}C), and high–temperature (>170 ^{o}C). The dielectric relaxations that occurred in these ranges are hereafter referred to as R_L, R_M, and R_H, respectively. To study dielectric relaxations in IN–T ceramics, the complex electric modulus (M*) was calculated from the complex dielectric permittivity (ε*) as follows:

$$M^* = M' + jM'' = 1/\varepsilon^* = 1/(\varepsilon' - j\varepsilon''), \quad (2)$$

where M′ and M″ are the real and imaginary parts of M*. ε′ and ε″ are the real (dielectric permittivity) and imaginary parts of ε*. The frequency dependence of M″ at various temperatures was investigated. At -20 ^{o}C [Fig. 5(a)], for the 10%IN–T sample, only one M″ peak was observed at ≈10^{3} Hz. A tail (a drastic increase in M″) in the high frequency range may signify another M″ peak corresponding to a low temperature dielectric response. However, this M″ peak could not be observed even at the lowest measurement temperature (-70 ^{o}C). This is not surprising, as reported by Zhao *et al.*[20], two low–temperature dielectric relaxations occurred in the case of 5%IN–T in the temperature range of 10–180 K (-260

to -93 ^{o}C). These two relaxations were also observed in the 0.5% (Ga+Nb) co–doped TiO_2 ceramic in the same temperature range.[29] Nevertheless, these low–temperature relaxations, R_L, are beyond the scope of the current study. At 20 °C [Fig. 5(b)], the apparent M″ peak shifted to a higher frequency. This set of relaxation peaks of M″ is very consistent with the tanδ peaks of the ambient RT dielectric relaxation [inset of Fig. 4(a)]. As demonstrated in Fig. 6(a), the frequencies at which M″ and tanδ peaks appeared at 0 ^{o}C are nearly in the same in position. This relaxation peak of M″ was clearly identified as R_M.

When the temperature was increased to 100 ^{o}C [Fig. 5(c)], no peak was observed. A tail in the low frequency range began to appear, which might have been R_H. M″ relaxation peaks appeared in a high temperature range (150–200 ^{o}C), as shown in Figs. 5(d)–(e). The M″ peak of R_H shifted to a high frequency as temperature was increased. The existence of R_H is reported in literature.[17] In the current study, only M″ peaks of R_M and R_H were observed in the 10%IN–T sample. The temperature dependences of these M″ peaks follow the Arrhenius equation, as is shown in Fig. 5(f). The relaxation activation energies for R_M and R_H of the 10%IN–T sample were, respectively, about 0.529 and 0.806 eV. It is observed that the activation energies of R_M obtained from tanδ and M″ were very close.

Considering R_M of the 10%IN–T sample, an application of this TiO_2–based material system in electronic devices might be difficult due to the temperature instability of ε′ in the vicinity of R_M. As shown in Fig. 6(b), R_M, which was indicated by a tanδ peak, was also observed in the 2.5%IN–T sample. The tanδ peak intensity and tanδ values over the measured frequency range of the 2.5%IN–T sample were lower than those of the 10%IN–T sample. In the point of view of application, these impressive dielectric properties (i.e., low tanδ and frequency–independent high–ε′) of the IN–T material system are of little value if this problem with R_M cannot be resolved.

The temperature–dependence of ε′ for 2.5% and 10%IN–T samples with significantly different dopant contents was determined. In Fig. 7(a), ε′ values of both samples seem to be independent of temperature over the range of -70 to 200 ^{o}C. However, careful inspection of the inset of Fig. 7(a) revealed large variations in ε′ for both samples as temperature was increased to more than 180 ^{o}C (>450 K). It is still impressive that ε′ greater than 10^4 with temperature independence to 180 ^{o}C is a notable achievement. In contrast to the 10%IN–T sample, the ε′ value of the 2.5%IN–T sample in a low temperature range was very slightly dependent on temperature. Notably, it was found that ε′ and tanδ of the 2.5%IN–T sample (at 30 ^{o}C and 10^2 Hz) were, respectively, $\approx 1.57\times10^4$ and ≈0.006. This extremely low tanδ value is especially impressive when compared to higher dopant content IN–T ceramics[17, 20] or other co–doped TiO_2 systems[23, 25, 29] as well as giant dielectric materials.[1, 8]

As seen in Fig. 7(b), the temperature coefficient of the 2.5%IN–T sample was as low as ±7 over a temperature range from -70 to 180 ^{o}C. This is satisfactory for X8R capacitor applications, in which ε′ of dielectric layers must not vary with temperature more than ±15% at temperatures between -55 and 150 ^{o}C. Compared to other X8R–based dielectric materials,[30-32] the more impressive properties of the 2.5%IN–T sample standout due to its much higher ε′ and extremely low tanδ values.

We now turn to briefly discuss the possible origin of R_M and R_H in the IN–T ceramic system to further develop better dielectric materials. The activation energies for R_M and R_H of the 10%IN–T sample were calculated and found to be ≈0.529–0.552 and 0.806 eV, respectively. Unfortunately, activation energy values of the 2.5%IN–T sample could not be calculated since only shoulder of M″relaxation peak was observed. Generally, the movement of oxygen vacancies in metal oxides occur at high temperatures and the required activation energies are generally quite high, e.g., 0.91 eV for $BaTiO_3$ ceramic[33] and 0.84–1.26 eV for

un–doped rutile TiO_2.[21] The activation energy of R_H is comparable to the values for the motion of oxygen vacancies. Thus, R_H is likely associated with oxygen vacancies. The slightly lower activation energy of the 10%IN–T ample may have been due to a greater number of oxygen vacancies caused by substitution of In^{3+} ions.

The activation energy of R_M was much larger than activation energies of ≈0.015–0.02 eV for polarization of free electrons in triangular shaped $In_2^{3+}V_O^{\bullet\bullet}Ti^{3+}$ defect complexes, which was suggested as the primary polarization giving rise to high dielectric performance of IN–T ceramics.[17] Interfacial polarization may be an important factor contributing to R_M. The activation energy of R_M is typically in the range of relaxation activation energy for electrical responses at the grain boundary, e.g., 0.55–0.6 eV for $CaCu_3Ti_4O_{12}$[3, 34] and 0.439eV for Li and Ti co–doped NiO.[8] Doping Nb^{5+} into TiO_2 can generate free electrons by reducing Ti^{4+} to Ti^{3+} as follows:

$$2TiO_2 + Nb_2O_5 \xrightarrow{4TiO_2} 2Ti'_{Ti} + 2Nb^{\bullet}_{Ti} + 8O_O + 1/2O_2, \quad (3)$$

$$Ti^{4+} + e \rightarrow Ti^{3+}. \quad (4)$$

Substitution of TiO_2 with In^{3+} required oxygen vacancies for charge compensation following the relation:

$$In_2O_3 \xrightarrow{2TiO_2} 2In'_{Ti} + V_O^{\bullet\bullet} + 3O_O. \quad (5)$$

Accordingly, several point defects were introduced in the rutile structure of co–doped samples. Two special local structures can be formed, triangular $In_2^{3+}V_O^{\bullet\bullet}Ti^{3+}$ and diamond $Nb_2^{5+}Ti^{3+}A_{Ti}$ (A=In^{3+}, Ti^{3+}, or Ti^{4+}) shapes.[17, 18] In principle, low tanδ coupled with high ε′ values can be obtained only in the cases of triangular and diamond shaped intrinsic–defect complexes that overlap or are strongly correlated. In practice, complete overlapping of these

two local structures is difficult (or perhaps impossible) to accomplished. Non−overlapped (or isolated) $Nb_2^{5+}Ti^{3+}A_{Ti}$ defect dipoles produce delocalized electrons, which is similar to the case of Nb^{5+}−doped TiO_2. Other free electrons are usually generated by oxygen loss during sintering process as follows:[20]

$$O_O^x \rightarrow \frac{1}{2}O_2 + V_O^{\bullet\bullet} + 2e' . \quad (6)$$

Under an applied electric field, hopping electrons are blocked by an insulating grain boundary and/or other internal interfaces, producing an additional interfacial polarization. Thus, R_M may have originated through interfacial polarization relaxation. With decreasing (In+Nb) co−dopant concentration, the number of delocalized electrons from the $Nb_2^{5+}Ti^{3+}A_{Ti}$ defect was possibly reduced. This can cause a decrease in interfacial polarization intensity. In the 2.5%IN−T sample, an additional ε′ value contributing from interfacial polarization should be less than that of the 10%IN−T sample. The deviation of the ε′ value at RT (contributed to by R_L+R_M) from the ε′ value in a relatively low−temperature range (arising from R_L alone) should be smaller in the case of the 2.5%IN−T sample. This resulted in lower values of the temperature coefficient at temperatures below RT.

As shown in Fig. 7(b), the positive and negative temperature coefficient values of both samples in the high and low temperature ranges, respectively, resulted from R_H and R_M. In the range of RT−150 ^oC, a significant difference in temperature dependent behaviors of the 2.5% and 10%IN−T samples appeared. Negative and positive coefficients were obtained in the 2.5% and 10% IN−T samples, respectively. A small positive coefficient of the 10%IN−T sample is similar to that reported earlier.[17] Interestingly, the negative value of the 2.5%IN−T sample has never been reported for co−doped TiO_2 materials and is similar to that of pure TiO_2, which was attributed to the dominant effect of ionic polarization. However, the ionic

polarization has never given rise to a ε′ value of more than 10^3 at RT. This result means that in addition to several dominant effects (i.e., electron–pinned defect–dipoles,[17] polaron hopping polarization,[20, 29] interfacial polarization,[20] and surface barrier layer[29] as well as the gradient in Ti^{3+} concentration distribution[27]), the dominant effect of ionic–like polarization caused by the introduction of various point defects may be another key factor that has a significant influence on the dielectric properties of co–doped TiO_2 materials. Intensive experimental and theoretical investigations are needed on this important topic.

4. Conclusions

IN–T ceramics were successfully synthesized using a SSR method. Highly dispersed In^{3+} and Nb^{5+} doping ions in the microstructure of IN–T ceramics were achieved. Substitution of these two ions resulted in an expansion of lattice parameters for both of *a* and *c* values. It was found that $\Delta C/C_{RT}$ values in low temperature (below RT) and high temperature (>150 ^oC) ranges of IN–T ceramics were primarily affected by R_M and R_H, respectively. R_H was associated with the movement on oxygen vacancies and found to be independent of dopant content. The R_M effect was dependent on co–dopant concentration and originated from interfacial polarization of delocalized charges. Highly co–doped 10%(In+Nb) substituted in TiO_2 resulted in extremely high ε′ values with very low tanδ, but failed to exhibit improved $\Delta C/C_{RT}$ values below RT due to the strong interfacial polarization effect. When the co–dopant content was decreased to 2.5%(In+Nb), the interfacial polarization effect was slight, leading a low $\Delta C/C_{RT}$ value of less than 5% in the temperature range from RT to -70 ^oC. Notably, a very high ε′ value of 1.57×10^4 and an ultra–low tanδ of ≈0.006 with an excellent temperature coefficient of less than ±7% in the range of -70–180 ^oC were achieved.

Acknowledgments

This work was financially supported by the Thailand Research Fund (TRF) and Khon Kaen University, Thailand [grant number RSA5880012]. W. Tuichai would like to thank the Thailand Graduate Institute of Science and Technology (TGIST) for his Master of Science Degree scholarship.

References

1. M. A. Subramanian, D. Li, N. Duan, B. A. Reisner and A. W. Sleight, *J. Solid State Chem.*, 2000, **151**, 323-325.
2. P. Lunkenheimer, R. Fichtl, S. Ebbinghaus and A. Loidl, *Phys. Rev. B*, 2004, **70**, 172102.
3. L. Liu, H. Fan, P. Fang and X. Chen, *Mater. Res. Bull.*, 2008, **43**, 1800-1807.
4. T. Park, Z. Nussinov, K. Hazzard, V. Sidorov, A. Balatsky, J. Sarrao, S. W. Cheong, M. Hundley, J.-S. Lee, Q. Jia and J. Thompson, *Phys. Rev. Lett.*, 2005, **94**, 017002.
5. S. Krohns, P. Lunkenheimer, C. Kant, A. V. Pronin, H. B. Brom, A. A. Nugroho, M. Diantoro and A. Loidl, *Appl. Phys. Lett.*, 2009, **94**, 122903.
6. P. Thongbai, T. Yamwong and S. Maensiri, *Mater. Lett.*, 2012, **82**, 244-247.
7. X. Q. Liu, B. W. Jia, W. Z. Yang, J. P. Cheng and X. M. Chen, *J. Phys. D: Appl. Phys.*, 2010, **43**, 495402.
8. Y.-H. Lin, M. Li, C.-W. Nan, J. Li, J. Wu and J. He, *Appl. Phys. Lett.*, 2006, **89**, 032907.
9. I. P. Raevski, S. A. Prosandeev, A. S. Bogatin, M. A. Malitskaya and L. Jastrabik, *J. Appl. Phys.*, 2003, **93**, 4130-4136.
10. Y. Y. Liu, X. M. Chen, X. Q. Liu and L. Li, *Appl. Phys. Lett.*, 2007, **90**, -.
11. N. Ikeda, H. Ohsumi, K. Ohwada, K. Ishii, T. Inami, K. Kakurai, Y. Murakami, K. Yoshii, S. Mori, Y. Horibe and H. Kito, *Nature*, 2005, **436**, 1136-1138.
12. C. Pecharromán, F. Esteban-Betegón, J. F. Bartolomé, S. López-Esteban and J. S. Moya, *Adv. Mater.*, 2001, **13**, 1541-1544.
13. J. Boonlakhorn, P. Thongbai, B. Putasaeng, T. Yamwong and S. Maensiri, *J. Alloys Compd.*, 2014, **612**, 103-109.

14. Z. Yang, L. Zhang, X. Chao, L. Xiong and J. Liu, *J. Alloys Compd.*, 2011, **509**, 8716-8719.

15. Y. Li, P. Liang, X. Chao and Z. Yang, *Ceram. Int.*, 2013, **39**, 7879-7889.

16. A. J. Moulson and J. M. Herbert, *Electroceramics : materials, properties, applications*, Wiley, West Sussex ; New York, 2nd edn., 2003.

17. W. Hu, Y. Liu, R. L. Withers, T. J. Frankcombe, L. Norén, A. Snashall, M. Kitchin, P. Smith, B. Gong, H. Chen, J. Schiemer, F. Brink and J. Wong-Leung, *Nat. Mater.*, 2013, **12**, 821-826.

18. C. C. Homes and T. Vogt, *Nat. Mater.*, 2013, **12**, 782-783.

19. J. Wu, C.-W. Nan, Y. Lin and Y. Deng, *Phys. Rev. Lett.*, 2002, **89**, 217601.

20. X.-g. Zhao, P. Liu, Y.-C. Song, A.-p. Zhang, X.-m. Chen and J.-p. Zhou, *Phys. Chem. Chem. Phys.*, 2015, **17**, 23132-23139.

21. C. Wang, N. Zhang, Q. Li, Y. Yu, J. Zhang, Y. Li and H. Wang, *J. Am. Ceram. Soc.*, 2015, **98**, 148-153.

22. S. Tangwancharoen, P. Thongbai, T. Yamwong and S. Maensiri, *Mater. Chem. Phys.*, 2009, **115**, 585-589.

23. Z. Li, J. Wu and W. Wu, *Journal of Materials Chemistry C*, 2015, **3**, 9206-9216.

24. Z. Gai, Z. Cheng, X. Wang, L. Zhao, N. Yin, R. Abah, M. Zhao, F. Hong, Z. Yu and S. Dou, *Journal of Materials Chemistry C*, 2014, **2**, 6790-6795.

25. X. Cheng, Z. Li and J. Wu, *Journal of Materials Chemistry A*, 2015, **3**, 5805-5810.

26. J. Li, F. Li, Y. Zhuang, L. Jin, L. Wang, X. Wei, Z. Xu and S. Zhang, *J. Appl. Phys.*, 2014, **116**, 074105.

27. W. Hu, K. Lau, Y. Liu, R. L. Withers, H. Chen, L. Fu, B. Gong and W. Hutchison, *Chem. Mater.*, 2015, **27**, 4934-4942.

28. M. N. Rahaman, *Ceramic processing and sintering*, M. Dekker, New York, 2nd edn., 2003.

29. W. Dong, W. Hu, A. Berlie, K. Lau, H. Chen, R. L. Withers and Y. Liu, *ACS Applied Materials & Interfaces*, 2015, DOI: 10.1021/acsami.5b07467.

30. Y. Sun, H. Liu, H. Hao, Z. Song and S. Zhang, *J. Am. Ceram. Soc.*, 2015, **98**, 1574-1579.

31. J. Jumpatam, B. Putasaeng, T. Yamwong, P. Thongbai and S. Maensiri, *J. Eur. Ceram. Soc.*, 2014, **34**, 2941-2950.

32. G. Yao, X. Wang, T. Sun and L. Li, *J. Am. Ceram. Soc.*, 2011, **94**, 3856-3862.

33. W. L. Warren, K. Vanheusden, D. Dimos, G. E. Pike and B. A. Tuttle, *J. Am. Ceram. Soc.*, 1996, **79**, 536-538.

34. T. B. Adams, D. C. Sinclair and A. R. West, *J. Am. Ceram. Soc.*, 2006, **89**, 3129-3135.

LIST OF FIGURE CAPTIONS

Fig. 1. (a) XRD pattern of $(In_{0.5}Nb_{0.5})_xTi_{1-x}O_2$ ceramics with x=0, 0.025, and 0.10. (b) Variation of lattice parameters of $(In_{0.5}Nb_{0.5})_xTi_{1-x}O_2$ ceramics with co–dopant concentration (x).

Fig. 2. SEM images of surface morphologies of $(In_{0.5}Nb_{0.5})_xTi_{1-x}O_2$ ceramics with (a) x=0.10 and (b) x=0.025.

Fig. 3. Element mapping of the $(In_{0.5}Nb_{0.5})_xTi_{1-x}O_2$ ceramic with x=0.025 sintered at 1550 ^oC for 1 h.

Fig. 4. (a) Frequency dependence of ε′ at various temperatures ranging from -60 to 180 ^oC for the $(In_{0.5}Nb_{0.5})_xTi_{1-x}O_2$ ceramic with x=0.1; inset shows tanδ at different temperatures. (b) Temperature dependence of ε′ and tanδ at various frequencies for the $(In_{0.5}Nb_{0.5})_xTi_{1-x}O_2$ ceramic with x=0.1. (c) Arrhenius plot of f_{max} for dielectric relaxation in (a) and (b). (d) Temperature coefficient of capacitance value at 1 kHz of the $(In_{0.5}Nb_{0.5})_xTi_{1-x}O_2$ ceramic with x=0.1.

Fig. 5. (a–e) M″ plots vs. of frequency at different temperatures. (f) Arrhenius plots for R_H and R_M.

Fig. 6. (a) Frequency dependence of tanδ and M″ at 0 ^oC for 2.5% IN–T. (b) Frequency dependence of tanδ at 0 ^oC for 2.5% IN–T and 10% IN–T ceramics.

Fig. 7. (a) Temperature dependence of ε′ at 1 kHz; inset shows ε′–temperature plots on a linear scale to clearly reveal the variation of ε′ over the measured temperature range. (b) Temperature coefficient of capacitance ($\Delta C/C_{30}$) at 1 kHz for 2.5% IN–T and 10% IN–T ceramics.

Fig. 1

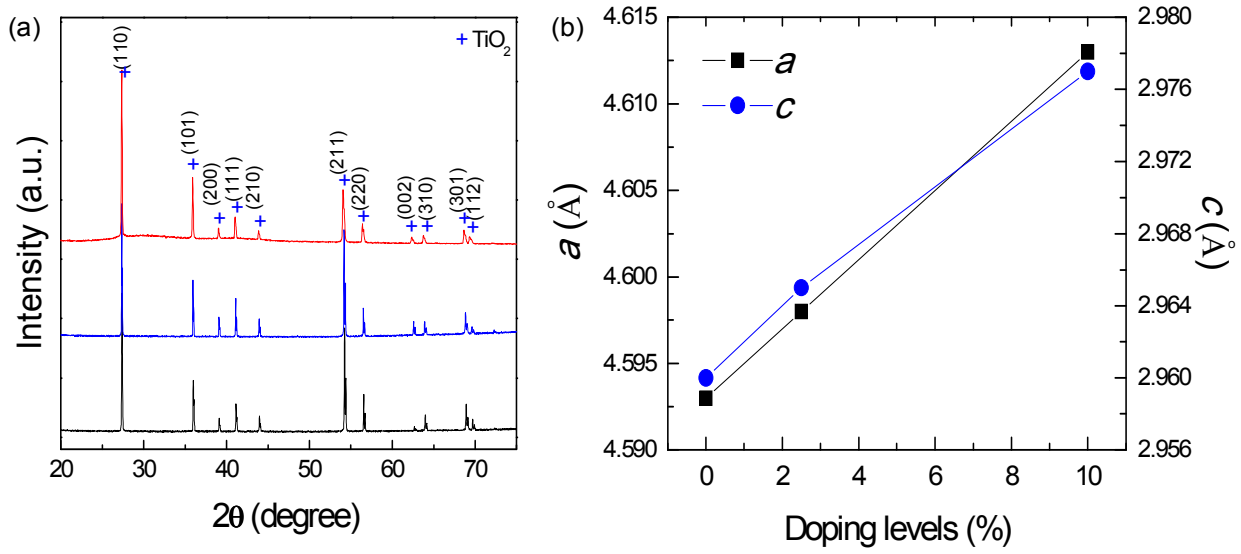

Fig. 2

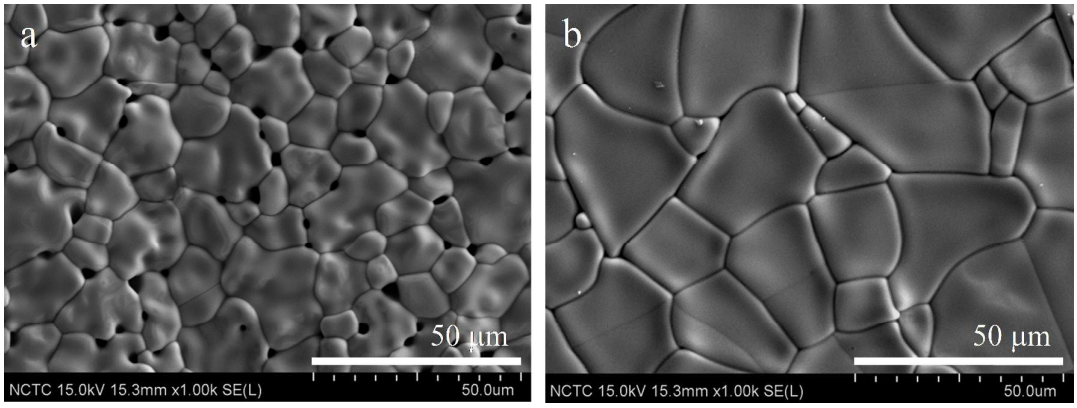

Fig. 3

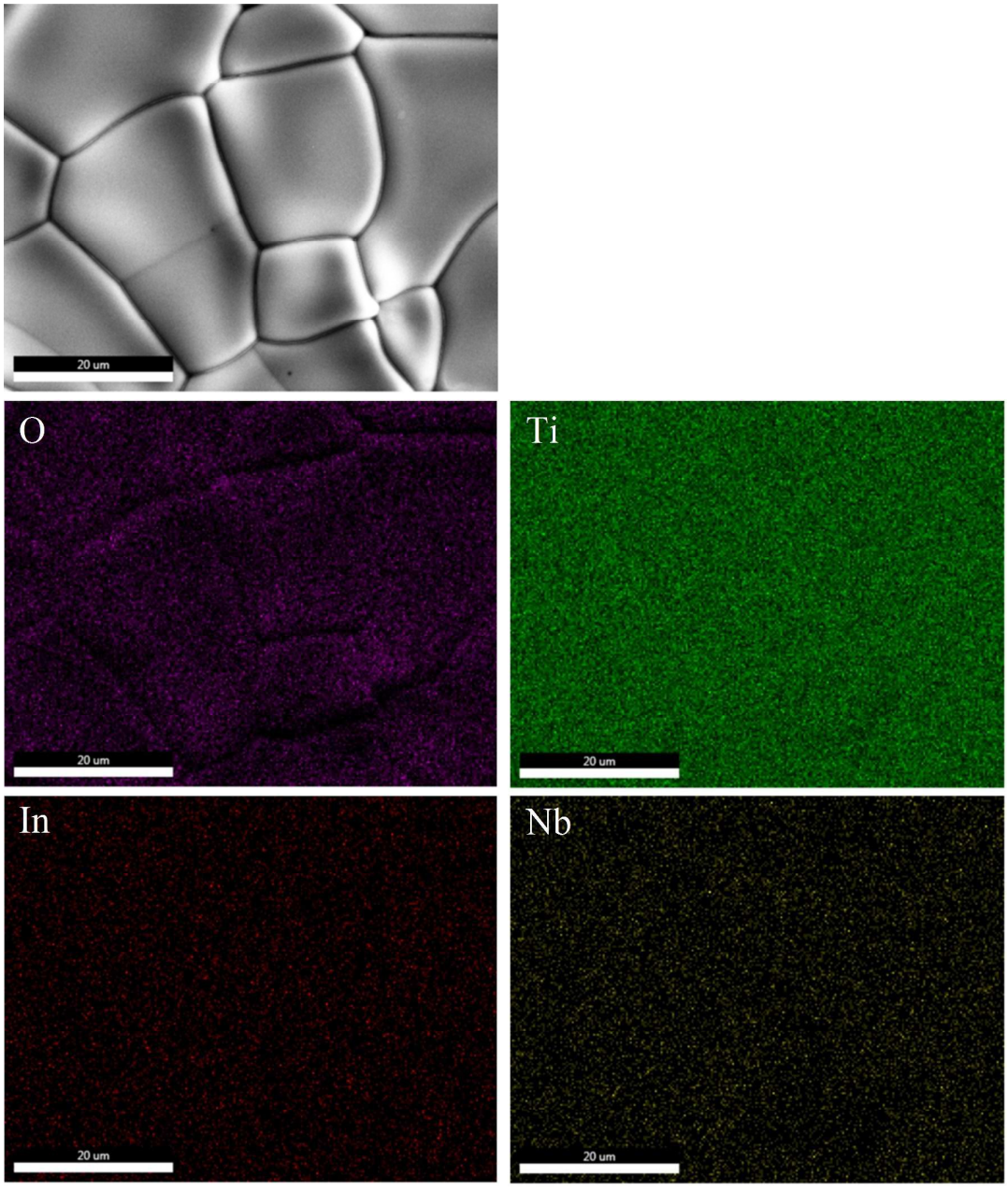

Fig. 4

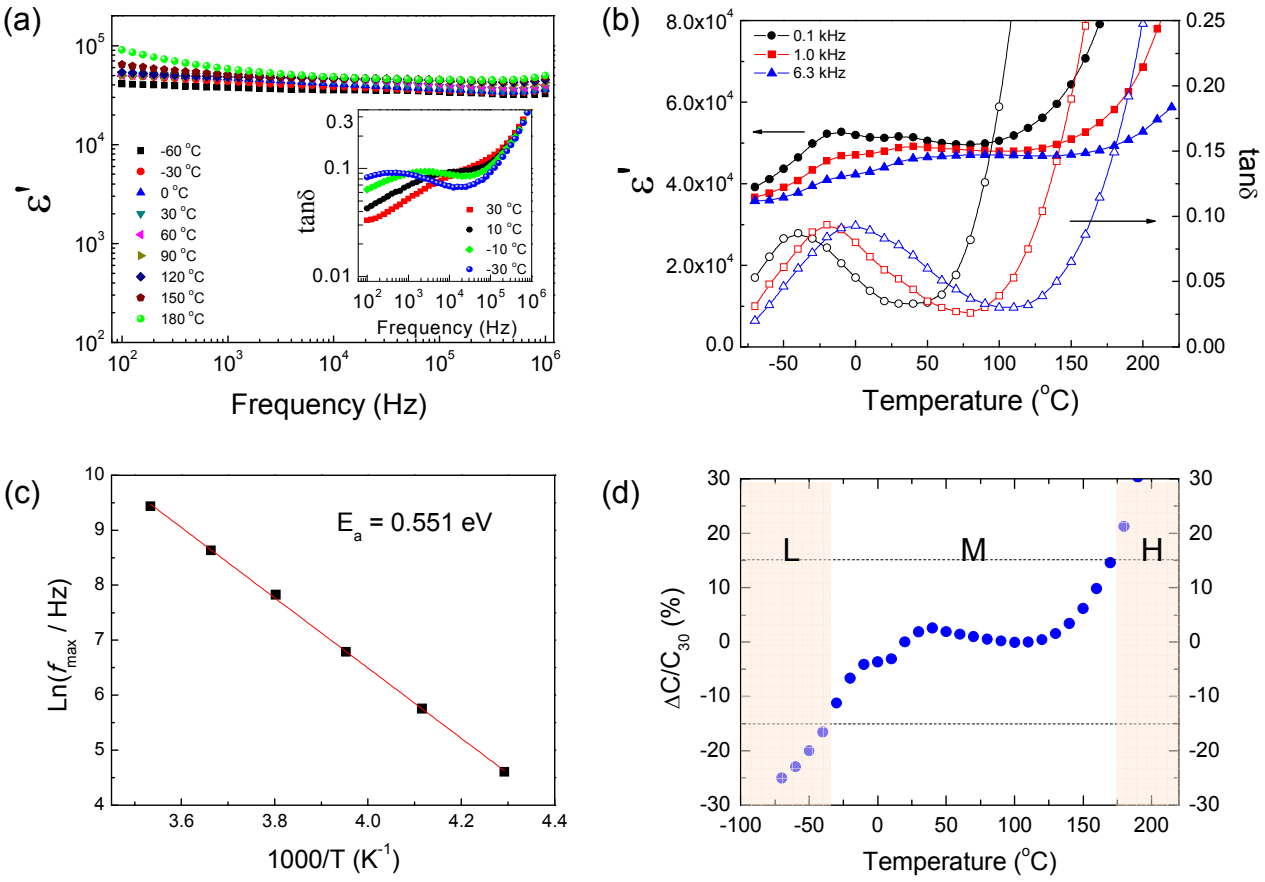

Fig. 5

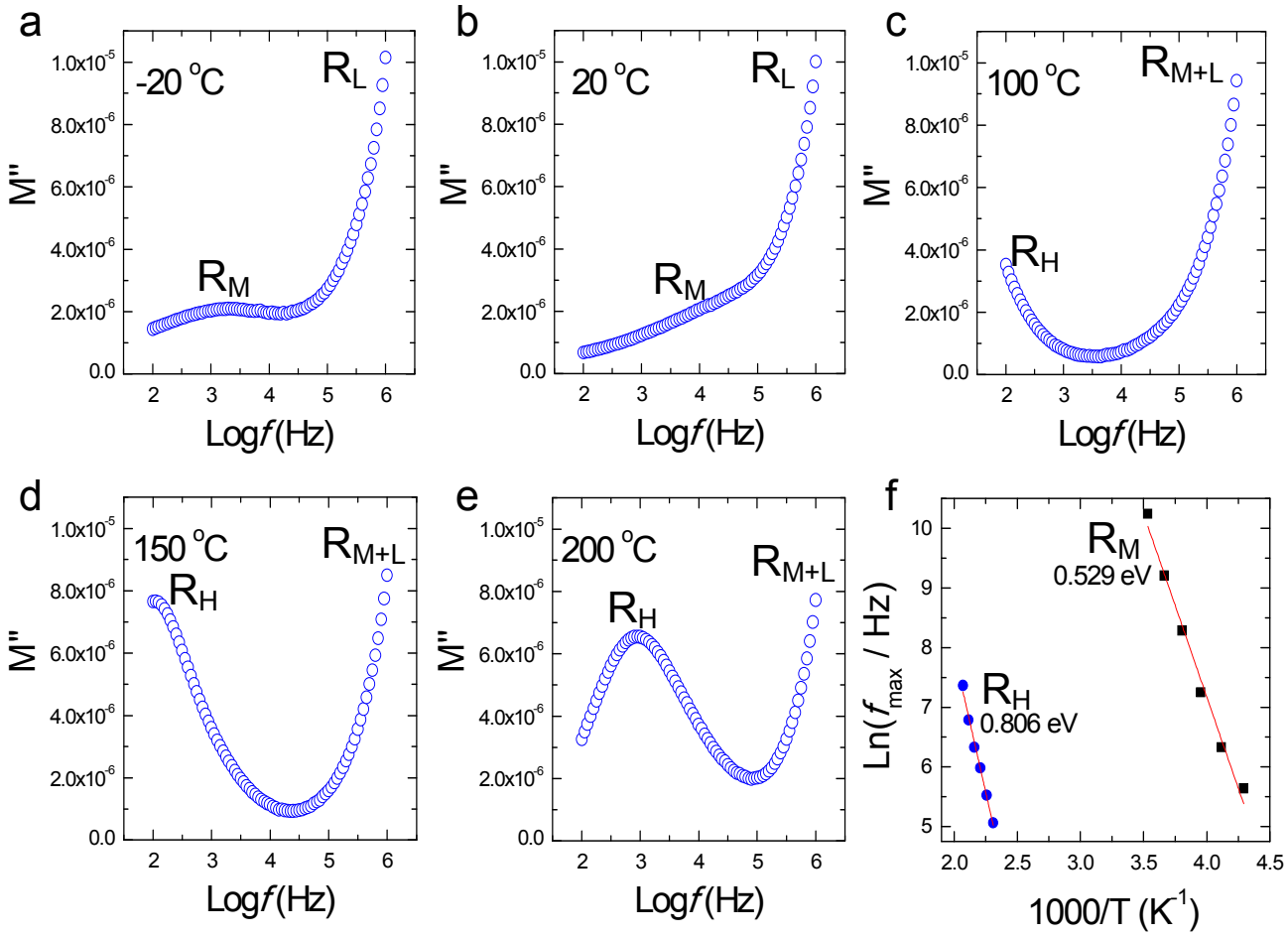

Fig. 6

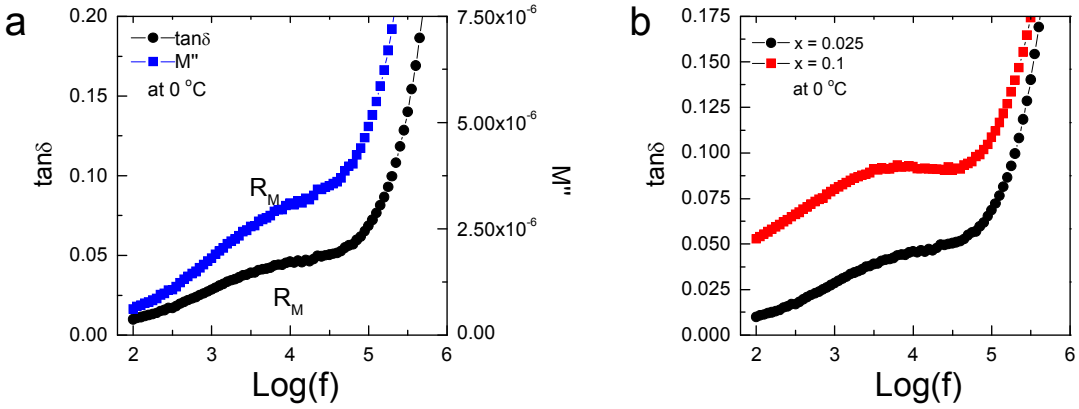

Fig. 7